BIOCHEMISTRY
including biophysical chemistry & molecular biology

Article

pubs.acs.org/biochemistry

New Determinants in the Catalytic Mechanism of Nucleoside Hydrolases from the Structures of Two Isozymes from *Sulfolobus solfataricus*

Claudia Minici,[†] Giovanna Cacciapuoti,[‡] Ester De Leo,[‡] Marina Porcelli,[‡] and Massimo Degano*[,†]

[†]Biocrystallography Unit, Department of Immunology, Transplantation, and Infectious Diseases, Scientific Institute San Raffaele, via Olgettina 58, 20132 Milan, Italy

[‡]Department of Biochemistry and Biophysics "F. Cedrangolo", Seconda Università di Napoli, Via Costantinopoli 16, 80138 Naples, Italy

Supporting Information

ABSTRACT: The purine- and pyrimidine-specific nucleoside hydrolases (NHs) from the archaeon *Sulfolobus solfataricus* participate in the fundamental pathway of nucleotide catabolism and function to maintain adequate levels of free nitrogenous bases for cellular function. The two highly homologous isozymes display distinct specificities toward nucleoside substrates, and both lack the amino acids employed for activation of the leaving group in the hydrolytic reaction by the NHs characterized thus far. We determined the high-resolution crystal structures of the purine- and pyrimidine-specific NHs from *S. solfataricus* to reveal that both enzymes belong to NH structural homology group I, despite the different substrate specificities. A Na^+ ion is bound at the active site of the pyrimidine-specific NH instead of the prototypical Ca^{2+}, delineating a role of the metals in the catalytic mechanism of NHs in the substrate binding rather than nucleophile activation. A conserved His residue, which regulates product release in other homologous NHs, provides crucial interactions for leaving group activation in the archaeal isozymes. Modeling of the enzyme−substrate interactions suggests that steric exclusion and catalytic selection underlie the orthogonal base specificity of the two isozymes.

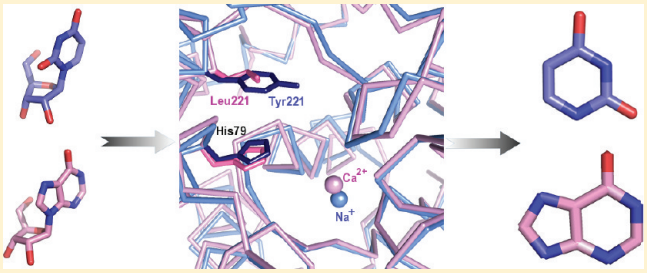

Nucleotides and their derivatives play a fundamental role in cellular metabolism, being used for short-term energy storage, for intra- and extracellular signaling, as enzyme cofactors, and for the synthesis of DNA and RNA. Living cells maintain adequate nucleotide levels through a delicate balance between de novo biosynthesis and salvage. Nucleosides are primarily intermediates in the catabolic pathway, and their conversion to mononucleotides proceeds through either phosphorylation by nucleoside kinases or the release of the base via the action of nucleoside phosphorylases (NPs) or nucleoside hydrolases (NHs) followed by the transfer of a phosphoribosyl moiety catalyzed by phosphoribosyltransferases (PRTases). NPs catalyze the phosphorolysis of the N-glycosidic bond in nucleosides to yield the free base and ribose 1-phosphate.[1] Their central role in nitrogenous base salvage in humans is evident from the immunodeficiency resulting from the lack of NP activity.[2] Inhibition of parasitic NPs could be an effective approach against pathogens that depend on nucleoside salvage, such as *Plasmodium falciparum*.[3]

NHs are glycosidases that catalyze the hydrolysis of the N-glycosidic bond of β-D-ribonucleosides to the corresponding free purine or pyrimidine base and ribose.[4] NH-encoding genes are conserved in all kingdoms of life, but notably absent in mammals. These enzymes have been characterized in protozoa,[5−8] bacteria,[9,10] yeast,[11] insects,[12] mesozoa,[13] plants,[14] and *Archaea*.[15,16] Four distinct subclasses of NHs can be inferred from the substrate preference: the nonspecific inosine-uridine NH (IU-NH),[7] the purine-specific inosine-adenosine-guanosine NH (IAG-NH),[5,8] the pyrimidine-specific cytidine-uridine NH (CU-NH),[10,17,18] and the 6-oxopurine-specific inosine-guanosine NH (IG-NH).[19,20] The physiological role of NHs is appreciated in purine-auxotrophic protozoan parasites such as trypanosomes, where they are essential in providing adequate supplies of purine bases for nucleotide biosynthesis.[21] On the other hand, the primary metabolic role of NHs in *Bacteria* and higher *Eukarya* is yet to be fully clarified. Indeed, NHs are apparently redundant in the nucleoside salvage of most organisms, substantially duplicating the NP activity but displaying 10−1000-fold lower specificity constants (k_{cat}/K_M) toward nucleoside substrates.[22] Existing functional data hint at highly specialized functions of NHs in different organisms, such as prevention of sporulation in *Bacillus cereus*,[23] host anesthetic in the mosquito *Aedes aegypti*,[12] and nicotinamide riboside-mediated maintenance of NAD^+ levels in yeast.[24] Enterobacterial NHs have also been proposed to act on uncommon

Received: September 2, 2011
Revised: May 2, 2012
Published: May 2, 2012

dx.doi.org/10.1021/bi300209g | *Biochemistry* 2012, 51, 4590−4599

substrates, including modified nucleosides found in tRNA and rRNA molecules.[10,17] A compelling issue in the field is whether a unifying physiological role of the NHs with different specificity could be defined, and the answer to such question requires a thorough characterization of these enzymes from different sources.

Sulfolobus solfataricus is a hyperthermophilic microorganism belonging to the *Archaea*,[25] the third evolutive line together with the well-known *Bacteria* and *Eukarya*. Hyperthermophilic *Archaea* are worthy of attention because of their capacity to survive and reproduce at temperatures near the boiling point of water[26] and are of extreme biotechnological interest not only because of the exceptional stability of their proteins[27,28] but also because of their unique enzymatic activities. Nucleoside salvage in *S. solfataricus* may proceed through reactions catalyzed by NPs and NHs. Two NPs have been isolated and characterized, SsMTAP[29,30] and SsMTAPII.[31,32] SsMTAP shows a broader substrate specificity, being able to utilize purine nucleosides and 5′-deoxy-5′-methylthioadenosine (MTA), while SsMTAPII can use only adenosine and MTA as substrates. Two NH-encoding genes are also present in *S. solfataricus*, encoding a pyrimidine-specific NH (SsCU-NH)[15] and a purine-preferring NH (SsIAG-NH).[16] These isozymes have 43% identical sequences and are apparently more homologous to the IU- and CU-NHs. Taken together, the enzymatic efficiencies of nucleobase-catabolizing enzymes in *S. solfataricus* suggest that under physiological conditions SsMTAP is the enzyme responsible for purine salvage, acting as a NP, while SsMTAPII is responsible for the catabolism of MTA.[31] Pyrimidine bases are apparently rescued exclusively via SsCU-NH, while SsIAG-NH could become relevant under particular environmental conditions such as starvation or oxidative stress, which could lead to a switch from a phosphorolytic to a hydrolytic catabolic pathway. Because of their evolutive differences and their unique physicochemical features, the structural and functional characterization of *Archaea* NHs could provide important information about the stability, mechanism of action, and substrate specificity of NHs.

We determined the crystal structures of SsIAG-NH and SsCU-NH to 1.8 and 1.6 Å resolution, respectively. Both enzymes are structurally similar to the IU- and CU-NHs, and their substrate specificities are dictated by a steric and catalytic selection of substrates. The crystal structure of SsCU-NH highlighted an unexpected substitution of the trademark active site Ca^{2+} by a Na^{+} ion, questioning the role of the active site metal in the enzymatic mechanism of NHs. Site-specific mutagenesis, sparked by the absence in the two SsNHs of the base-activating residues found in other previously characterized NH enzymes, demonstrated an unanticipated role of a conserved His residue in catalysis, providing evidence of alternative means of leaving group stabilization in this intriguing class of enzymes.

MATERIALS AND METHODS

Bacterial Strains, Plasmid, Enzymes, and Chemicals. *Escherichia coli* strain BL21(λDE3) was purchased from Novagen (Darmstadt, Germany). Plasmid pET-22b(+) and the NucleoSpin Plasmid kit for plasmid DNA preparation were obtained from Genenco (Duren, Germany). Specifically synthesized oligodeoxyribonucleotides were obtained from MWG-Biotech (Ebersberg, Germany). Restriction endonucleases and DNA-modifying enzymes were obtained from Takara Bio, Inc. (Otsu, Shiga, Japan). *Pfu* DNA polymerase was purchased from Stratagene (La Jolla, CA). Nucleosides, purine and pyrimidine bases, and standard proteins used in molecular mass studies were obtained from Sigma (St. Louis, MO). Isopropyl β-D-thiogalactoside was from Applichem (Darmstadt, Germany). All reagents were of the purest commercial grade.

Mutagenesis of SsIAG-NH, Protein Expression, and Purification. The site-specific His79Ala SsIAG-NH mutant was generated by site-directed mutagenesis using the QuickChange kit (Stratagene). The *SsIAG-NH* gene SSO2243 (GenBank accession number AE006829.1) cloned into the pET-22b(+) expression vector was used as a template. Primers for site-directed mutagenesis were designed according to the instructions for the QuickChange kit. Mutation was confirmed by DNA sequence analysis. The purified plasmid was used for transformation of *E. coli* BL21(λDE3) cells, and protein expression was induced as previously described.[16]

All the purification steps were performed at room temperature. Cells (10 g) were enzymatically lysed, and the cell debris was removed by centrifugation at 20000*g* for 60 min at 4 °C. The mutant SsIAG-NH was readily purified to homogeneity through a fast and efficient two-step procedure that utilizes a heat treatment followed by affinity chromatography on 5′-methylthioinosine-Sepharose.[16] Protein concentrations were determined through the Bradford method using bovine serum albumin as the standard. Protein eluting from the columns during purification was monitored as absorbance at 280 nm. The concentration of the His79Ala SsIAG-NH mutant enzyme was estimated spectrophotometrically using an ε_{280} of 51910 M^{-1} cm^{-1}. The subunit molecular mass and protein homogeneity were determined by sodium dodecyl sulfate−polyacrylamide gel electrophoresis.

Enzyme Assay and Determination of Kinetic Constants. NH activity was determined following the formation of purine/pyrimidine base from the corresponding nucleoside by high-performance liquid chromatography using a Beckman system Gold apparatus as previously described.[16] In all kinetic assays, the amount of protein was adjusted so that no more than 10% of the substrate was converted to product and the reaction rate was strictly linear as a function of time and protein concentration.

Homogeneous preparations of His79Ala SsIAG-NH were used for steady-state kinetic analysis. The enzymatic reaction rate was linear for at least 10 min at 80 °C; thus, an incubation time of 5 min was employed for kinetic experiments. All enzyme reactions were performed in triplicate. The kinetic K_M and V_{max} values were obtained from linear regression analysis of data fit to the Michaelis−Menten equation. Values are averages from at least three experiments with standard errors. The k_{cat} value was calculated by dividing V_{max} by the total enzyme concentration and considering four independent active sites per tetramer.

Quaternary Structure Analysis. Analytical size exclusion chromatography was performed using a Superdex 200 10/30 column coupled to a AktaPurifier10 FPLC system (GE Healthcare). Proteins were eluted isocratically at a flow rate of 0.5 mL/min with a buffer containing 20 mM Bis-Tris (pH 5.5) and 100 mM NaCl. Dynamic light scattering measurements were performed with a DynaPro MS-X instrument, optimizing laser intensity and exposure time to prevent detector saturation.

Protein Crystallization. SsIAG-NH was expressed and purified as previously described.[16] The purified protein at a concentration of 4−8 mg/mL in storage buffer [10 mM Tris

dx.doi.org/10.1021/bi300209g | *Biochemistry* 2012, 51, 4590−4599

Table 1. Data Collection and Structure Refinement Statistics

	SsIAG-NH	SsCU-NH
	Data Collection[a]	
cell parameters	a = 84.76 Å, b = 81.13 Å, c = 98.02 Å, β = 100.70°	a = 194.94 Å, b = 194.94 Å, c = 42.86 Å
space group	$P2_1$	$P6_422$
wavelength (Å)	0.933	0.976
resolution range (Å)	100−1.8 (1.9−1.8)	100−1.6 (1.7−1.6)
no. of measured reflections	582529 (86828)	1643327 (199539)
no. of unique reflections	119836 (17747)	63505 (10373)
redundancy	4.9 (4.9)	25.9 (19.2)
completeness (%)	99.1 (98.5)	99.9 (100)
R_{sym}[b]	0.087 (0.619)	0.070 (0.32)
$\langle I/\sigma(I)\rangle$	14.7 (2.9)	73.3 (11.9)
	Refinement	
resolution range (Å)[a]	96.23−1.8 (1.85−1.8)	100−1.6 (1.64−1.6)
no. of reflections, $F(hkl) > 0$	113799	60312
no. of atoms per asymmetric unit	10757	2646
R_{crys}[c]	0.170 (0.241)	0.156 (0.155)
R_{free}[d]	0.214 (0.282)	0.170 (0.160)
rmsd for bonds (Å)	0.016	0.016
rmsd for angles (deg)	1.479	1.399
average B factor (Å^2)[e]	25.1, 35.4	30.3, 27.3
Ramachandran statistics[f]	97.6, 0.2	97.8, 0.0

[a]The numbers in parentheses refer to data for the highest-resolution shell. [b]$R_{sym} = \sum_{hkl}\sum_i|I_i(hkl) - \langle I(hkl)\rangle|/\sum_{hkl}\sum_i I_i(hkl)$. [c]$R_{crys} = \sum_{hkl}||F_o(hkl)| - |F_c(hkl)||/\sum_{hkl}|F_o(hkl)|$. [d]$R_{free}$ is the same as R_{crys} but calculated on a randomly selected subset of reflections (5%) excluded from all stages of refinement (6036 for SsIAG-NH and 3224 for SsCU-NH). [e]Average temperature factors for protein and solvent atoms, respectively. [f]Percentages of residues in favored and disallowed regions of a Ramachandran plot, respectively, computed using MOLPROBITY.[40]

(pH 7.4)] was crystallized using the hanging drop vapor diffusion method, mixing 1 μL of protein and 1 μL of a precipitant solution consisting of 100 mM Hepes (pH 7.5), 5% PEG 3350, 5 mM $CaCl_2$, 5 mM $CdCl_2$, and 5 mM $MgCl_2$. A single crystal was harvested and cryoprotected by sequential transfer into stabilizing solutions consisting of 100 mM Hepes (pH 7.5), 5% PEG 3350, 5 mM $CaCl_2$, 5 mM $CdCl_2$, 5 mM $MgCl_2$, and a concentration of glycerol increasing from 5 to 20%. The crystal was flash-cooled and maintained in liquid nitrogen until data were collected.

SsCU-NH was expressed and purified as described elsewhere.[15] After purification, the protein was dialyzed and stored in a buffer consisting of 20 mM Bis-Tris (pH 5.5) and 100 mM NaCl at a concentration of 4−8 mg/mL. The pyrimidine-specific enzyme was crystallized using the hanging drop vapor diffusion method by mixing an equal amount of protein and a precipitant solution, composed of 100 mM bicine (pH 9) and 1.5 M ammonium sulfate. A single crystal was harvested and cryoprotected by consecutive dipping into stabilizing solutions consisting of 100 mM bicine (pH 9), 1.5 M ammonium sulfate, and a concentration of sodium malonate increasing from 10 to 40%. The crystal was flash-cooled in liquid nitrogen and maintained at cryogenic temperatures until data were collected.

Data Collection, Structure Solution, and Refinement. Diffraction data were collected at beamlines ID14-EH1 (SsIAG-NH) and ID23-1 (SsCU-NH) of the European Synchrotron Radiation Facility (ESRF Grenoble, France) using the oscillation method at 100 K. For the SsCU-NH, diffraction data were collected in two passes, yielding high- and low-resolution data sets, and ensuring an overlap between the two data sets to allow accurate scaling of the intensities. Data were indexed, integrated, scaled, and reduced to unique reflections using XDS.[33] Space group assignment was performed on the basis of the intensities of symmetry-related reflections, systematic absences, and best solution in the translation function. The measured intensities were converted to structure factor amplitudes using TRUNCATE.[34] Initial phases were obtained with the molecular replacement method as implemented in MOLREP.[35] For SsIAG-NH, the search model was the CfIU-NH monomer [Protein Data Bank (PDB) entry 2MAS] after truncation of all non-Gly residues to alanine and removal of solvent molecules, ions, and ligands. For the SsCU-NH, the search model was the refined SsIAG-NH polypeptide. After the search models had been positioned, the structures were built and the amino acid sequence was assigned using ARP/wARP.[36] The models underwent cycles of restrained energy minimization with a maximum likelihood target function using REFMAC5[37] followed by manual rebuilding into σ_A-weighted electron density maps with COOT.[38] For the SsIAG-NH, noncrystallographic symmetry restraints were applied to avoid overrefinement, as judged from the divergence between the R_{crys} and R_{free} validators. For the SsCU-NH, anisotropic motion was modeled by refinement of the TLS parameters.[39] Solvent molecules were added using ARP/wARP in spherical residual density peaks greater than 3σ. The stereochemical quality of the models was continuously analyzed with MOLPROBITY[40] to identify regions requiring manual intervention. Details of data quality and final refinement and Ramachandran statistics are listed in Table 1. Figures were prepared using CHIMERA[41] and PYMOL (The PyMOL Molecular Graphics System, version 0.99rc6, Schrödinger, LLC).

Substrate Docking. The models of liganded NHs were obtained using AUTODOCK version 4.2.[42] The protein models were the monomeric unligated structures of SsIAG-NH and SsCU-NH after removal of water molecules and fortuitous ligands, but keeping the active site ions. The ligand inosine was taken from the structure in complex with YeiK

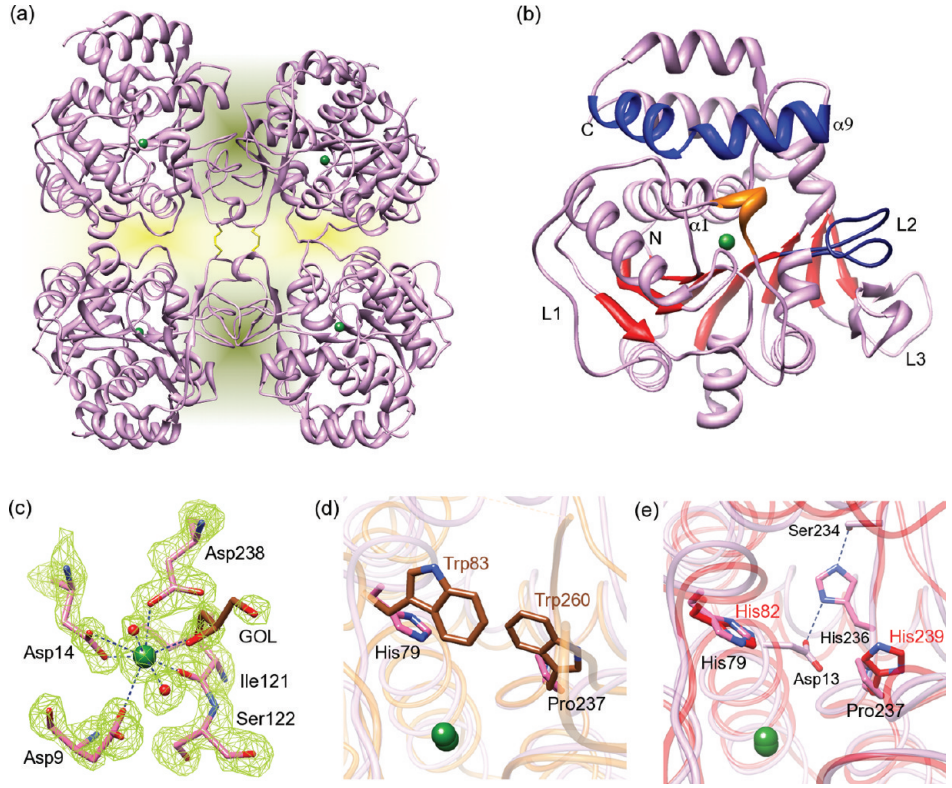

Figure 1. Structure and active site of the SsIAG-NH. (a) Cartoon representation of the homotetrameric assembly of the SsIAG-NH. The major and minor interaction surfaces involved in the quaternary structure assembly are shaded green and yellow, respectively. The disulfide bridges are highlighted in yellow. (b) Structure of the SsIAG-NH monomer. Ordered secondary structure elements are depicted as arrows (β-strands) or helical segments (α-helices), and the active site Ca^{2+} is shown as a green sphere. The core β-sheet is colored red, and helix α9 and the L2 region, bordering the active site, are colored blue. The L1 region harboring residue His79 is colored orange. (c) Ca^{2+} ion binding site. The active site ion is shown as a green sphere; the chelating residues are shown as sticks and ordered water molecules as red spheres. The electron density map shown is a σ_A-weighted "shake" omit map calculated with ($|F_o| - |F_c|$, ϕ_c) coefficients after the residues shown had been omitted from the model, and applying a random shift to the remaining atoms to a final rmsd of 0.25 Å. (d) Active site differences between SsIAG-NH and TvIAG-NH. Residues His79 and Pro237 of SsIAG-NH (carbon atoms colored pink) occupy the same positions in space as residues Trp83 and Trp260 of TvIAG-NH (carbon atoms colored brown), where they activate the leaving purine base through aromatic stacking. (e) Active site differences between SsIAG-NH and *E. coli* CU-NH YeiK. Residue His239 in YeiK (carbon atoms colored red) superimposes with Pro237 of SsIAG-NH. His236 in SsIAG-NH is hydrogen bonded to Asp13 and Ser234, hindering its relocation toward the inside of the active site.

(PDB entry 3B9X[43]), while a uridine molecule was built on the basis of the conformation of the inhibitor bound to YbeK (PDB entry 3G5I[44]). For both nucleosides, the ribose was kept in the C4′-endo puckered conformation, as commonly found in ribosides bound to NHs. The nucleoside molecules allowed for torsional flexibility around the C2′−O2′, C3′−O3′, C5′−O5′, and N-glycosidic bonds. The NH structures allowed for the side chain flexibility of the following residues: Asp13, Val78, His79, Asn155, Phe162, Trp186, and Tyr224 for the SsIAG-NH and Asp13, Val78, His79, Asn156, Phe163, Trp187, Tyr221, and Tyr224 for the SsCU-NH. The active site boundaries were defined as the minimum rectangular box encompassing all flexible residues and the active site ions. For both ligands and enzymes, polar hydrogens were added, and Gasteiger charges were computed. Three hundred runs of docking using a Lamarckian genetic algorithm were computed for each ligand−enzyme pair. Results were analyzed using ADT4.[42]

RESULTS

The Crystal Structure of the SsIAG-NH Reveals a Group I-like Structure. We crystallized the SsIAG-NH in the absence of added ligands and determined its structure to a resolution of 1.8 Å (Table 1). The molecular replacement technique was used to determine initial phases, and the procedure was readily successful when either IU- or CU-NHs were used as search models. The protein crystallized as a homotetramer in the crystal asymmetric unit, displaying the quaternary structure that is characteristic of IU- and CU-NHs (Figure 1a). Indeed, despite a shared substrate specificity, the SsIAG-NH differs in tertiary and quaternary structure from the *Trypanosoma vivax* (Tv) IAG-NH. The rmsd with the *E. coli* CU-NH YeiK is 1.46 Å for 289 homologous Cα atoms, compared to 1.77 Å over 268 Cα atoms with the TvIAG-NH (Figure S1 of the Supporting Information). The SsIAG-NH attains its homotetrameric structure through association of two different monomer−monomer interfaces, a minor surface defined by the N-terminal portion of the loop connecting strand β3 to helix α3 (L1), helix α4, and helix α5, and a major surface composed of residues from the loop connecting β5 to α5 (L2) and the long segment connecting β7 to β9 (L3). In tetrameric NHs, the interaction between the major surfaces leads to the largest decrease in dimerization free energy, as calculated using the PISA server. However, the presence in the SsIAG-NH of a covalent disulfide bond connecting monomer A to B and monomer C to D (as per PDB file nomenclature) confers the highest computed stability to the minor interface.

dx.doi.org/10.1021/bi300209g | *Biochemistry* 2012, 51, 4590−4599

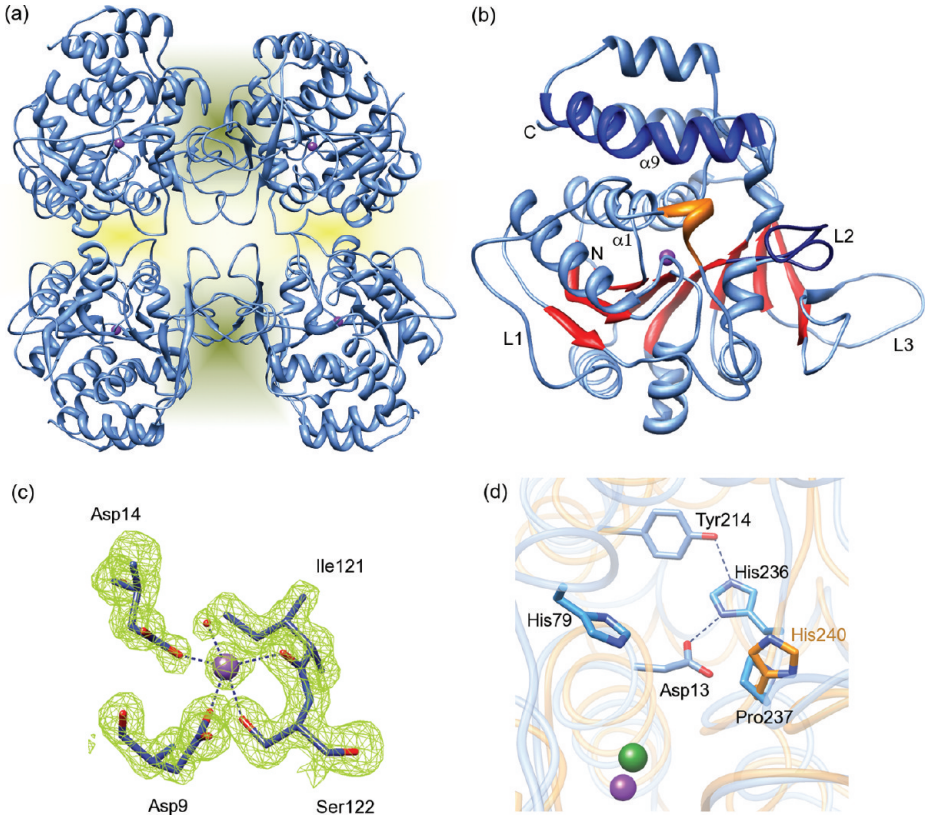

Figure 2. Structure and active site of SsCU-NH. (a) Cartoon representation of the homotetrameric assembly of the SsCU-NH. The major and minor interaction surfaces involved in the quaternary structure assembly are shaded green and yellow, respectively. (b) Structure of the SsCU-NH monomer. Segments are colored as in Figure 1. The active site Na^+ ion is shown as a violet sphere. (c) Na^+ ion binding site. The active site ion is shown as a violet sphere, and the chelating residues are shown as sticks. The electron density map shown is a σ_A-weighted "shake" omit map calculated as described in the legend of Figure 1. (d) Active site comparison with the *E. coli* CU-NH YbeK. His240 of YbeK (carbon atoms colored orange) superimposes with Pro237 of the SsCU-NH (carbon atoms colored blue). His236 of the SsCU-NH interacts via hydrogen bonds with residues Asp13 and Tyr214. The Na^+ ion lies deeper in the active site pocket compared to the corresponding Ca^{2+} of YbeK.

The structure of the individual subunit resembles the NH fold (Figure 1b), with a central mixed β-sheet composed of seven parallel strands and one antiparallel strand flanked by six α-helices.[45,46] The active site is lined by the L1 loop (residues 75−81) and the C-terminal portion of helix α9 (residues 223−229), which are readily identified in electron density maps, and their average temperature factors are close to the value observed for all protein atoms (for instance, 25.9 $Å^2$ vs 20.1 $Å^2$ in chain A), thus indicating their low degree of flexibility. This finding is in contrast with those of other unliganded NH enzymes so far characterized, where these segments are highly flexible and undergo a structural reorganization as substrate-mimicking ligands enter the active site, establishing contacts with the base moiety.[46,47] The stabilization of these structures in SsIAG-NH can be ascribed either to the presence of two glycerol molecules derived from the cryoprotection buffer bound to the active site, as observed for the *E. coli* CU-NH YeiK,[17] or to the extensive intramolecular interactions of amino acid residues in the L1 loop with helices α9 and α1.

The SsIAG-NH active site contains the trademark Ca^{2+} ion of NH enzymes, octacoordinated by residues Asp9, Asp14, Ile121, and Asp238, two solvent molecules, and one glycerol molecule (Figure 1c). The base-interacting portion of the active site of the SsIAG-NH is surprisingly devoid of the side chains that typically activate the leaving group in NHs. Indeed, the SsIAG-NH lacks the Trp residue found in the TvIAG-NH (Trp260) involved in aromatic stacking with the purine base[48] (Figure 1d). A structural homologue of the trademark His (His241 in the CflU-NH and His239 in the *E. coli* YeiK) that transfers a proton to the substrate aglycone in the reactions catalyzed by IU- and CU-NHs[49] is also absent (Figure 1e). These amino acids are located in the short β-strand following helix α9 that flanks the active site and are immediately followed by an Asp residue involved in Ca^{2+} chelation. In SsIAG-NH, this position is occupied by Pro237, immediately preceded by a His residue in the amino acid sequence. The His236 residue of SsIAG-NH points away from the active site cavity and establishes hydrogen bonds with Asp13 and Ser234 within the core of the protein, conferring a substantial rigidity to the region (Figure 1e). It is thus unlikely that this residue would undergo a substantial rearrangement upon substrate binding to participate in leaving group protonation. Hence, the only putative proton-donating residue at the SsIAG-NH active site is His79, a strictly conserved amino acid in IU- and CU-NHs that is known to regulate the substrate-induced conformational change in the enterobacterial NH YeiK.[47]

The Crystal Structure of the SsCU-NH Reveals a Unique Na^+ Ion at the Active Site. The SsCU-NH structure was determined to a resolution of 1.6 Å (Table 1). The protein crystallized as a monomer in the asymmetric unit, but the characteristic group I NH tetrameric structure is obtained through crystallographic 222 symmetry (Figure 2a). Indeed, both size exclusion chromatography and dynamic light scattering measurements at concentrations of 114 and 228

dx.doi.org/10.1021/bi300209g | *Biochemistry* 2012, 51, 4590−4599

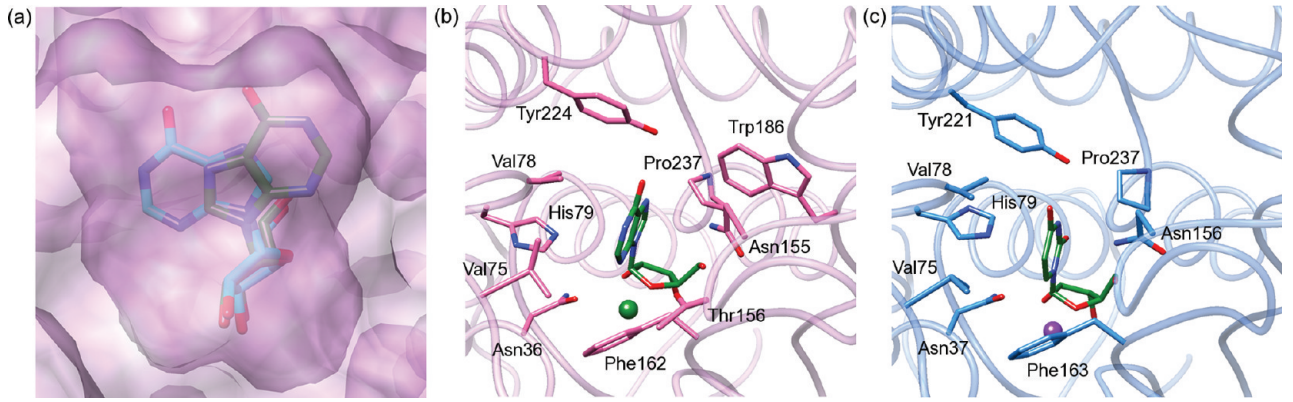

Figure 3. Models of the enzyme–substrate interactions for the SsIAG-NH and SsCU-NH. (a) Molecular surface of the SsIAG-NH active site (rendered as semitransparent and colored pink) with an inosine molecule shown as sticks with the purine base oriented either as observed in the *E. coli* YeiK enzyme (carbon atoms colored green) or in a nearly opposite orientation (carbon atoms colored cyan). Both orientations are compatible with the active site volume. (b) Inosine bound to the active site of SsIAG-NH in the same conformation as in YeiK, as obtained through flexible docking. Residues within 4.5 Å of the nitrogenous base are shown as sticks. (c) Model of a uridine molecule bound to the SsCU-NH. Residues within 4.5 Å of the pyrimidine base are shown as sticks.

μM (not shown) indicate a tetrameric quaternary structure. The SsCU-NH subunit retains the overall structure of the orthologue NHs (Figure 2b), displaying an rmsd of 1.6 Å for 290 structurally equivalent Cα atoms with the *E. coli* CU-NH YbeK[18,44] and 1.6 Å for 299 Cα atoms with the *Crithidia fasciculata* (Cf) IU-NH (Figure S2 of the Supporting Information). The SsIAG-NH and SsCU-NH are highly homologous in tertiary structure (rmsd of 1.0 Å for 293 structurally equivalent Cα atoms), with the largest differences found in the L1 and L3 regions (Figure S3 of the Supporting Information). This structural divergence is reflected in the solvent-accessible surface areas buried upon tetramer formation, 1424 and 674 Å^2 in SsCU-NH compared to 1188 and 693 Å^2 in SsIAG-NH. As seen for the purine-specific isozyme, the SsCU-NH crystallized with both the L1 loop (residues 75–81) and C-terminal end of helix α9 (residues 223–229) clearly structured despite the absence of either specific or fortuitous active site ligands. This finding suggests that, in striking contrast with what was observed for the structures of NHs determined so far, at low temperatures the closed structure of SsNHs is stabilized by intramolecular contacts. An increase in flexibility, required for access to the active site by the substrate and catalysis, may be achieved through the thermal energy available at the archaeon physiological temperature.

Remarkably, the electron density map of SsCU-NH indicated the presence of an ion at the active site differing from the canonical Ca^{2+}, because its refinement leads to the appearance of a negative residual electron density peak at this position. The density was ascribed to a Na^+ ion based on its pentacoordination geometry, ligating group nature (oxygen atoms), and distances (between 2.2 and 2.4 Å). Moreover, the refined *B* factor of a Na^+ ion is closely correlated with the ligating atoms, and no residual difference electron density is apparent. The ion is shifted by 1.41 Å compared to the position of Ca^{2+} in the SsIAG-NH toward the bottom of the active site pocket and is coordinated by the side chains of residues Asp9, Asp14, and Ser122, the main chain carbonyl of Ile121, and an ordered water molecule (Figure 2c). Notably, residue Ser122 is present also in the purine-specific SsIAG-NH enzyme, but in this enzyme, the side chain hydroxyl adopts a different conformation and does not participate in the coordination of the Ca^{2+} ion (Figure 1c).

We further investigated whether this crystallographic finding could be otherwise confirmed. The kinetic properties of the SsCU-NH enzyme are unaffected by addition of Ca^{2+} (not shown). The presence of Na^+ is not caused by the purification protocol, which is identical for the SsIAG-NH. To exclude the possibility that the ion was displaced in the crystallization process, we determined the structure of the SsCU-NH in a different crystal form obtained using polyethylene glycol as a precipitant. This second crystal structure presents the same active site geometry and composition (data not shown). Finally, to exclude a possible effect of the different pH values of the storage buffer in promoting the presence of Na^+, we measured the catalytic activity of the enzyme both in the storage buffer and at the same pH of the crystallization buffer. No differences in activity were observed compared to the measurements at neutral pH, thus suggesting that the protein was crystallized in the active form, and that a Na^+ ion is likely bound to the enzyme under physiological conditions. This unique feature of the SsCU-NH can be ascribed to the presence of residue Glu12, an amino acid residue never previously encountered in NHs at this position. The side chain carboxylate of Glu12 is within 2.7 Å of the imidazole moiety of His79, fostering a strong interaction that leads to a shift of helix α1 compared to other NHs. This helix bears the metal-chelating residue Asp14, and the reorganization of the ion binding environment favors the specific interaction with monovalent alkali ions.

As already observed in SsIAG-NH, the active site of SsCU-NH does not harbor the characteristic His residue involved in base protonation in IU- or CU-NHs. As observed in SsIAG-NH, this position is occupied by a Pro residue (Figure 2d). Thus, a different amino acid side chain must be involved in neutralizing the negative charge developing at the pyrimidine ring during catalysis.

Modeling of Enzyme–Substrate Interactions in the *S. solfataricus* NHs. The structures of the two archaeal NHs were determined in the absence of specific, substrate-mimicking ligands. Soaking or cocrystallization with iminoribitol-based compounds, known inhibitors of other NHs, also did not yield crystals with an occupied active site. Hence, we resorted to modeling and docking studies to understand the determinants for the different substrate specificities of the two enzymes. We used the highly similar structure of YeiK in complex with

dx.doi.org/10.1021/bi300209g | *Biochemistry* 2012, 51, 4590–4599

Table 2. Kinetic Parameters of NHs and Their Mutants[a]

	k_{cat} (s^{-1})	K_M (μM)	k_{cat}/K_M ($\times 10^4$ s^{-1} M^{-1})
SsIAG-NH	11.6 ± 0.4	340 ± 20	3.41 ± 0.23
His79Ala SsIAG-NH	0.85 ± 0.025	326 ± 20	0.26 ± 0.02
CfIU-NH	44 ± 3	150 ± 40	29 ± 8
His241Ala CfIU-NH	0.021 ± 0.0005	530 ± 260	0.0039 ± 0.0019
YeiK	4.7 ± 0.1	142 ± 8	3.3 ± 0.2
H82N YeiK	15.5 ± 1.1	345 ± 55	4.5 ± 0.8

[a]Steady-state kinetic parameters of the *S. solfataricus* IAG-NH and its point mutant His79Ala for inosine substrate. For comparison, the kinetic data for the *C. fasciculata* IU-NH and its His241Ala mutant for the same substrate are reported.[49] In addition, the kinetic data for the *E. coli* CU-NH YeiK and its His82Asn mutant for the substrate uridine are reported.[17] The effect of the His82Asn mutation on the hydrolysis of uridine by the *E. coli* CU-NH YeiK is negligible, consistent with a minor role of the His residue in proton transfer in the enterobacterial enzyme.

inosine (PDB entry 3B9X)[43] to model by structural superposition a purine nucleoside at the SsIAG-NH active site. The ribose was kept in the C4′-endo conformation, as observed in the structures of liganded IU- and CU-NHs so far determined. In the model, the atoms of the ribosyl moiety closely superimpose with a glycerol and one water molecule. The SsIAG-NH active site pocket has a volume larger than that of YeiK (759 and 454 $Å^3$, respectively), a consequence of the conformation of the L1 loop and C-terminal portion of helix α9, and of the smaller side chains of the helix α9 residues protruding into the active site cavity (Gln227 and His239 in YeiK and Thr226 and Pro237 in SsIAG-NH). Taken together, these differences allow the base moiety of purine nucleoside substrates to potentially assume either the same orientation that is observed in YeiK ($\chi = -52°$, dihedral angle defined by atoms O4′, C1′, N9, and C4) or a nearly opposite one ($\chi = 114°$) (Figure 3a). Other base orientations, such as the anti conformation of the purine ring observed in the TvIAG-NH in complex with the transition-state-like inhibitor immucillin H (PDB entry 2FF2),[50] cannot be attained in the SsIAG-NH because of severe steric clashes with the side chains of Val78 and His79. To resolve this conundrum of the purine base orientation, we resorted to in silico flexible docking. More than 40% of the docked molecules assume a conformation of the nitrogenous base consistent with what was observed in the YeiK−inosine complex,[43] while the opposite conformation was not significantly represented. The active site Ca^{2+} ion is octacoordinated by the protein ligands and the two ribosyl O2′ and O3′ hydroxyls. The purine ring of the substrate establishes van der Waals' contacts with residues Asn36, Val75, Val78, His79, Asn155, Thr156, Phe162, Trp186, and Pro237. The side chain of Tyr224 can extend to form a favorable hydrogen bond interaction with the O6 carbonyl of the base (Figure 3b).

The SsCU-NH shows the highest degree of structural and functional similarity to the *E. coli* protein YbeK; hence, we superimposed the structure of this CU-specific enzyme in complex with an iminoribitol-based inhibitor (PDB entry 3G5I)[44] to model a molecule of uridine at the active site. To independently validate the model, we used flexible docking to confirm the correctness of the binding mode of the pyrimidine nucleoside. The presence of a Na^+ rather than the typical Ca^{2+} ion results in a different binding network between the substrate and the protein. The ligand enters deeper into the active site pocket; the O2′ hydroxyl replaces the Na^+-coordinating solvent molecule, while the O3′ hydroxyl is more than 3.0 Å from the ion. The O2′ hydroxyl can establish polar interactions with the side chains of Asp9 and Asn37 and O3′ those with the Ile121 carbonyl oxygen and side chain amide of Asn164. Finally, O5′ is within hydrogen bonding distance of Asn156, Glu162, and the main chain nitrogen of Phe163. The base moiety is stabilized by polar interactions between the O4 carbonyl and the amide nitrogen of Asn156 and between the N3 nitrogen and the imidazole ring of His79 and by van der Waals contacts with Asn37, Val75, Val78, His79, Asn156, Phe163, Tyr221, and Pro237 (Figure 3c). In particular, residue Tyr221 closely approaches the O2 carbonyl of the pyrimidine ring.

A Novel Proton Donor in SsNH-Catalyzed Nucleoside Hydrolysis. Remarkably, both *S. solfataricus* enzymes lack both the His and the Trp residue at the active site (replaced by a Pro in the two isozymes), and no other aromatic residues are positioned to promote an aromatic stacking interaction. The only ionizable amino acid side chain pointing toward the substrate binding cavity in the SsNHs that could protonate the leaving group is the His79 residue. This residue is present in all known CU- and IU-NHs and has been implicated in triggering the conformational change that takes place upon substrate binding and product release.[47]

To establish a possible role of His79 in the leaving group activation of the *S. solfataricus* NHs, we engineered a His79Ala mutant of the SsIAG-NH. The mutant SsIAG-NH gene was overexpressed in *E. coli* and the recombinant protein purified following the same procedure that was used for the wild-type enzyme,[16] and its steady-state kinetic parameters were determined. Steady-state kinetic analysis of this mutant using inosine as a substrate revealed a 13.7-fold decrease in k_{cat}, while the K_M value was unmodified (Table 2). Similarly, unchanged values of K_M and 9- and 20-fold decreases in k_{cat} were observed with adenosine and guanosine, respectively (data not shown). This variation in k_{cat} is not comparable to the decrease observed for the CfIU-NH upon mutation of the proton-transferring residue His241[49] and may be thus be ascribed to a conformational change in the enzyme. However, the effect is remarkably similar to that observed for the Trp260Ala mutation in the TvIAG-NH, where product release is rate-limiting.[50] Supporting the role of His79 in leaving group stabilization, the mutation of this His residue in the highly homologous CU-NH YeiK leads to increases in both V_{max} and K_M[17] (Table 2). We conclude that His79 participates in the catalytic mechanism of the archaeal NHs, likely acting as the proton donor to facilitate the departure of the nitrogenous base.

DISCUSSION

Although several enzymes with NH activity have been so far characterized at both the structural and functional level, previous studies of the purine-specific and pyrimidine-specific isozymes from the archaeon *S. solfataricus* identified peculiar features in substrate specificity that warranted further structural and biophysical characterization. In this work, we report the

determination of the high-resolution structures of the SsIAG-NH and SsCU-NH that ultimately shed light on the determinants of substrate specificity and identify a yet unanticipated role of a conserved His in the catalytic mechanism.

The structure and mechanism of action of NHs belonging to different specificity classes are well-characterized,[4,46,51] yet the two NHs from the hyperthermophilic *S. solfataricus* revealed novel, unexpected features. First, both enzymes belong to structural homology group I of tetrameric NHs that does not include purine-specific isozymes. The SsIAG-NH hence differs from the trypanosomal TvIAG-NH in kinetic properties,[5] quaternary structure, and active site residues involved in substrate binding and leaving group activation. The most striking active site feature in the SsIAG-NH is the absence of the aromatic residues that in the TvIAG-NH activate the leaving group through a stacking interaction with the purine ring, thus indicating a distinct mechanism for substrate selection and catalysis. Not surprisingly, the catalytic efficiency (k_{cat}/K_M) of SsIAG-NH toward inosine is more similar to that of the structurally homologous CfIU-NH,[16,51] and it is ∼100-fold lower than in TvIAG-NH[5] toward all purinic substrates, mostly because of the higher K_M values (Table S1 of the Supporting Information). Remarkably, the SsIAG-NH cannot exploit the same mechanism for purine ring protonation of IU- or CU-NHs, as it lacks all members of the catalytic triad involved in the transfer of the proton to the base,[43] including the prototypical His241 (according to the numbering in the CfIU-NH). Instead, site-specific mutagenesis of the archaeal SsIAG-NH demonstrated that residue His79 mediates the leaving group activation. Interestingly, this residue is conserved in both IU- and CU-NHs and has a known role in modulating substrate entry and catalysis in the CU-NH YeiK[47] but does not participate in substrate protonation.[17] Hence, in light of these results, it is apparent that His79 can play a dual role in the catalytic mechanism of NHs, modulating substrate entry and product release in the isozymes bearing a homologue of the CfIU-NH His241 residue or acting as a proton donor in the ones that lack the aforementioned residue such as SsNHs. Thus, NH enzymes evolved with at least two different mechanisms for the activation of the purine leaving group in the hydrolytic reaction in the context of two divergent active sites, aromatic stacking or protonation. However, two different His residues from distinct structural elements may participate in the latter mechanism in isozymes from different sources. A mechanism similar to that presented here for the archaeal NHs may be also postulated for the NHs from pluricellular organisms previously identified[17] whose sequences lack a homologue of His241, substituted with a conserved Cys, but maintain the His79 residue.

The active site of the SsCU-NH revealed an unexpected feature compared to the other NHs, as it lacks the bivalent Ca^{2+} ion at the ribosyl-binding moiety of the active site. The binding of a Na^+ ion at the SsCU-NH active site is preferred because of the presence of a unique Glu residue, whose interactions with the side chain of His79 lead to an active site structure that ultimately favors the binding of the Na^+ over the prototypical Ca^{2+} ion. The kinetic parameters of the Na^+-containing SsCU-NH do not differ substantially from those of other group I NHs. For instance, the catalytic efficiency toward pyrimidine nucleosides of the SsCU-NH (Table S1 of the Supporting Information) is comparable with that of YeiK.[15,17] These results hence suggest that the active site cation in NHs is cardinal for maintaining the active site structure and geometry, where three facing Asp residues that bind the ribosyl moiety of the nucleoside substrates require a counterion for stabilization. A role of the metal in the binding of substrates is also evident, because one or two ribosyl hydroxyls of the bound nucleoside complete the ion coordination. However, because of their different charge densities, alkali and alkaline earth metals are expected to distinctly affect the acidity of the catalytic water that is part of the ion coordination sphere. It remains to be determined whether these differences in nucleophile pK_a also influence the transition state of the enzymatic reaction. Ab initio calculations may provide a quantitative assessment of the polarization of the incoming water molecule in both situations.

The SsIAG-NH and SsCU-NH enzymes share a remarkably similar active site composition, yet they differ in substrate specificity. The structures here reported lack substrate analogues, but their similarity with other NHs allows the identification of the amino acid residues that may participate in binding and catalytic interactions. In SsCU-NH, the conformation of the C-terminal portion of helix α9 and L2 closely approaching the ligand (Figure 4) and the presence of the side chains of Tyr221 and Ile231 cause an overall reduction in the volume of the active site (511 Å^3) compared to that of the SsIAG-NH (759 Å^3). Binding of purine nucleosides would require a conformational adjustment of the active site to prevent unfavorable steric clashes with the base, thus reducing the enzymatic efficiency of SsCU-NH toward these substrates. Instead, the considerably higher catalytic efficiency of the SsIAG-NH for purine over pyrimidine nucleosides (>10^3) is likely imposed both at the binding and at the catalytic level. Indeed, residue His79 is adequately positioned for the direct transfer of a proton to the N7 atom of the purine ring in the SsIAG-NH-catalyzed reaction, but not to the O2 carbonyl of uridine, for instance. In the SsCU-NH, the amino acid Tyr221 is instead within hydrogen bonding distance of the O2 carbonyl of the modeled uridine molecule. This interaction may compensate for the negative charge developing at the transition state of the hydrolysis of pyrimidine nucleosides, as proposed for the enterobacterial isozymes.[18] In the purine-specific NH, a

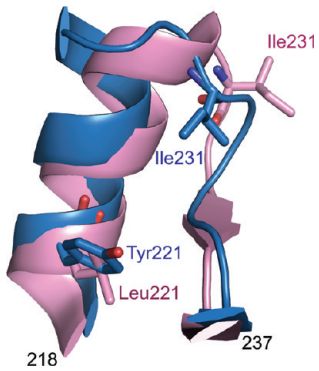

Figure 4. Comparison of the active sites of SsIAG-NH and SsCU-NH. The region encompassing helix α9, the following loop, and a short β-strand lining the NH active site is shown in a ribbon representation for SsIAG-NH (pink) and SsCU-NH (light blue). Residue Tyr221 in the SsCU-NH protrudes toward the binding cavity, and its homologue in the SsIAG-NH is a Leu. In the SsCU-NH, the loop assumes a more "closed" conformation, and the side chain of Ile231 occupies the upper portion of the active site, likely preventing adequate binding of the larger purine nucleosides.

dx.doi.org/10.1021/bi300209g | *Biochemistry* 2012, 51, 4590−4599

Tyr221 homologue is not present, and this difference is likely responsible for the marginal activity on pyrimidine nucleoside substrates, providing an unfavorable environment for both substrate binding and turnover of pyrimidine nucleosides by SsIAG-NH. Indeed, a recent mutagenesis study (M. Porcelli et al., manuscript in press) showed that a SsIAG-NH with an engineered Leu221Tyr/Asn228Val double mutation is able to catalyze the hydrolysis of uridine, underscoring the importance of this aromatic residue in determining substrate specificity.

CONCLUSIONS

The crystal structures of two NH isozymes from the archaeon *S. solfataricus* provide new insights into the catalytic mechanism of these N-glycosidases, demonstrating that alternative proton donors may be employed in the process of leaving group activation in tetrameric NHs. The presence of a Na^+ ion bound to the SsCU-NH active site, unanticipated and never previously reported for NH enzymes, suggests a structural role of the metals in maintaining the correct geometry for optimal interactions with the substrates. A limited set of amino acid substitutions modulates the specificity of the two isozymes, underscoring the plasticity of the NH fold in adapting to the chemical features of the physiological substrates.

ASSOCIATED CONTENT

Supporting Information

Kinetic comparison of different NHs and superpositions of the SsNHs with structural homologues. This material is available free of charge via the Internet at http://pubs.acs.org.

Accession Codes

Coordinates and structure factors have been deposited in the Protein Data Bank as entries 3T8I (SsIAG-NH) and 3T8J (SsCU-NH).

AUTHOR INFORMATION

Corresponding Author

*E-mail: degano.massimo@hsr.it. Phone: +39-022643-7152. Fax: +39-022643-4153.

Funding

Supported by grants from Fondazione Cariplo NOBEL, Italian Basic Research Funding (FIRB), "Regione Campania" L.R. n.5/2007, and "Ministero dell'Università e della Ricerca Scientifica" Prin 2007.

Notes

The authors declare no competing financial interest.

ACKNOWLEDGMENTS

We acknowledge the use of beamlines ID23-1 and ID14-EH1 at the European Synchrotron Radiation Facility for data collection.

ABBREVIATIONS

NH, nucleoside hydrolase; IAG-NH, inosine-, adenosine-, and guanosine-preferring NH (purine-specific NH); CU-NH, cytidine- and uridine-preferring NH (pyrimidine-specific NH); IU-NH, inosine- and uridine-preferring NH (nonspecific NH); IG-NH, inosine- and guanosine-preferring NH (6-oxopurine-specific NH); MTA, 5′-deoxy-5′-methylthioadenosine; MTAP, MTA phosphorylase; NP, nucleoside phosphorylase; PRTase, phosphoribosyl transferase; rmsd, root-mean-square deviation.

REFERENCES

(1) Pugmire, M. J., and Ealick, S. E. (2002) Structural analyses reveal two distinct families of nucleoside phosphorylases. *Biochem. J. 361*, 1−25.

(2) Seegmiller, J. E., Watanabe, T., Shreier, M. H., and Waldmann, T. A. (1977) Immunological aspects of purine metabolism. *Adv. Exp. Med. Biol. 76A*, 412−433.

(3) Kicska, G. A., Tyler, P. C., Evans, G. B., Furneaux, R. H., Schramm, V. L., and Kim, K. (2002) Purine-less death in *Plasmodium falciparum* induced by immucillin-H, a transition state analogue of purine nucleoside phosphorylase. *J. Biol. Chem. 277*, 3226−3231.

(4) Versees, W., and Steyaert, J. (2003) Catalysis by nucleoside hydrolases. *Curr. Opin. Struct. Biol. 13*, 731−738.

(5) Versees, W., Decanniere, K., Pelle, R., Depoorter, J., Brosens, E., Parkin, D. W., and Steyaert, J. (2001) Structure and function of a novel purine specific nucleoside hydrolase from *Trypanosoma vivax*. *J. Mol. Biol. 307*, 1363−1379.

(6) Shi, W., Schramm, V. L., and Almo, S. C. (1999) Nucleoside hydrolase from *Leishmania major*. Cloning, expression, catalytic properties, transition state inhibitors, and the 2.5-Å crystal structure. *J. Biol. Chem. 274*, 21114−21120.

(7) Parkin, D. W., Horenstein, B. A., Abdulah, D. R., Estupinan, B., and Schramm, V. L. (1991) Nucleoside hydrolase from *Crithidia fasciculata*. Metabolic role, purification, specificity, and kinetic mechanism. *J. Biol. Chem. 266*, 20658−20665.

(8) Miller, R. L., Sabourin, C. L., Krenitsky, T. A., Berens, R. L., and Marr, J. J. (1984) Nucleoside hydrolases from *Trypanosoma cruzi*. *J. Biol. Chem. 259*, 5073−5077.

(9) Ogawa, J., Takeda, S., Xie, S. X., Hatanaka, H., Ashikari, T., Amachi, T., and Shimizu, S. (2001) Purification, characterization, and gene cloning of purine nucleosidase from *Ochrobactrum anthropi*. *Appl. Environ. Microbiol. 67*, 1783−1787.

(10) Petersen, C., and Moller, L. B. (2001) The RihA, RihB, and RihC ribonucleoside hydrolases of *Escherichia coli*. Substrate specificity, gene expression, and regulation. *J. Biol. Chem. 276*, 884−894.

(11) Magni, G., Fioretti, E., Ipata, P. L., and Natalini, P. (1975) Bakers' yeast uridine nucleosidase. Purification, composition, and physical and enzymatic properties. *J. Biol. Chem. 250*, 9−13.

(12) Ribeiro, J. M., and Valenzuela, J. G. (2003) The salivary purine nucleosidase of the mosquito, *Aedes aegypti*. *Insect Biochem. Mol. Biol. 33*, 13−22.

(13) Versees, W., Van Holsbeke, E., De Vos, S., Decanniere, K., Zegers, I., and Steyaert, J. (2003) Cloning, preliminary characterization and crystallization of nucleoside hydrolases from *Caenorhabditis elegans* and *Campylobacter jejuni*. *Acta Crystallogr. D59*, 1087−1089.

(14) Abusamhadneh, E., McDonald, N. E., and Kline, P. (2000) Isolation and characterization of adenosine nucleosidase from yellow lupin (*Lupinus luteus*). *Plant Sci. 153*, 25−32.

(15) Porcelli, M., Concilio, L., Peluso, I., Marabotti, A., Facchiano, A., and Cacciapuoti, G. (2008) Pyrimidine-specific ribonucleoside hydrolase from the archaeon *Sulfolobus solfataricus*: Biochemical characterization and homology modeling. *FEBS J. 275*, 1900−1914.

(16) Porcelli, M., Peluso, I., Marabotti, A., Facchiano, A., and Cacciapuoti, G. (2009) Biochemical characterization and homology modeling of a purine-specific ribonucleoside hydrolase from the archaeon *Sulfolobus solfataricus*: Insights into mechanisms of protein stabilization. *Arch. Biochem. Biophys. 483*, 55−65.

(17) Giabbai, B., and Degano, M. (2004) Crystal structure to 1.7 Å of the *Escherichia coli* pyrimidine nucleoside hydrolase YeiK, a novel candidate for cancer gene therapy. *Structure 12*, 739−749.

(18) Muzzolini, L., Versees, W., Tornaghi, P., Van Holsbeke, E., Steyaert, J., and Degano, M. (2006) New insights into the mechanism of nucleoside hydrolases from the crystal structure of the *Escherichia coli* YbeK protein bound to the reaction product. *Biochemistry 45*, 773−782.

(19) Estupinan, B., and Schramm, V. L. (1994) Guanosine-inosine-preferring nucleoside N-glycohydrolase from *Crithidia fasciculata*. *J. Biol. Chem. 269*, 23068−23073.

(20) Vandemeulebroucke, A., Minici, C., Bruno, I., Muzzolini, L., Tornaghi, P., Parkin, D. W., Versees, W., Steyaert, J., and Degano, M. (2010) Structure and mechanism of the 6-oxopurine nucleosidase from *Trypanosoma brucei brucei*. *Biochemistry 49*, 8999−9010.
(21) Hammond, D. J., and Gutteridge, W. E. (1984) Purine and pyrimidine metabolism in the *Trypanosomatidae*. *Mol. Biochem. Parasitol. 13*, 243−261.
(22) Belenky, P., Christensen, K. C., Gazzaniga, F., Pletnev, A. A., and Brenner, C. (2009) Nicotinamide riboside and nicotinic acid riboside salvage in fungi and mammals. Quantitative basis for Urh1 and purine nucleoside phosphorylase function in NAD^+ metabolism. *J. Biol. Chem. 284*, 158−164.
(23) Todd, S. J., Moir, A. J., Johnson, M. J., and Moir, A. (2003) Genes of *Bacillus cereus* and *Bacillus anthracis* encoding proteins of the exosporium. *J. Bacteriol. 185*, 3373−3378.
(24) Belenky, P., Racette, F. G., Bogan, K. L., McClure, J. M., Smith, J. S., and Brenner, C. (2007) Nicotinamide riboside promotes Sir2 silencing and extends lifespan via Nrk and Urh1/Pnp1/Meu1 pathways to NAD. *Cell 129*, 473−484.
(25) Woese, C. R., Kandler, O., and Wheelis, M. L. (1990) Towards a natural system of organisms: Proposal for the domains Archaea, Bacteria, and Eucarya. *Proc. Natl. Acad. Sci. U.S.A. 87*, 4576−4579.
(26) Mozhaev, V. V., Berezin, I. V., and Martinek, K. (1988) Structure-stability relationship in proteins: Fundamental tasks and strategy for the development of stabilized enzyme catalysts for biotechnology. *CRC Crit. Rev. Biochem. 23*, 235−281.
(27) Vieille, C., and Zeikus, G. J. (2001) Hyperthermophilic enzymes: Sources, uses, and molecular mechanisms for thermostability. *Microbiol. Mol. Biol. Rev. 65*, 1−43.
(28) Sterner, R., and Liebl, W. (2001) Thermophilic adaptation of proteins. *Crit. Rev. Biochem. Mol. Biol. 36*, 39−106.
(29) Cacciapuoti, G., Porcelli, M., Bertoldo, C., De Rosa, M., and Zappia, V. (1994) Purification and characterization of extremely thermophilic and thermostable 5′-methylthioadenosine phosphorylase from the archaeon *Sulfolobus solfataricus*. Purine nucleoside phosphorylase activity and evidence for intersubunit disulfide bonds. *J. Biol. Chem. 269*, 24762−24769.
(30) Appleby, T. C., Mathews, I. I., Porcelli, M., Cacciapuoti, G., and Ealick, S. E. (2001) Three-dimensional structure of a hyperthermophilic 5′-deoxy-5′-methylthioadenosine phosphorylase from *Sulfolobus solfataricus*. *J. Biol. Chem. 276*, 39232−39242.
(31) Cacciapuoti, G., Forte, S., Moretti, M. A., Brio, A., Zappia, V., and Porcelli, M. (2005) A novel hyperthermostable 5′-deoxy-5′-methylthioadenosine phosphorylase from the archaeon *Sulfolobus solfataricus*. *FEBS J. 272*, 1886−1899.
(32) Zhang, Y., Porcelli, M., Cacciapuoti, G., and Ealick, S. E. (2006) The crystal structure of 5′-deoxy-5′-methylthioadenosine phosphorylase II from *Sulfolobus solfataricus*, a thermophilic enzyme stabilized by intramolecular disulfide bonds. *J. Mol. Biol. 357*, 252−262.
(33) Kabsch, W. (1988) Automatic indexing of rotation diffraction patterns. *J. Appl. Crystallogr. 21*, 67−72.
(34) French, S., and Wilson, K. (1978) On the treatment of negative intensity observations. *Acta Crystallogr. A34*, 517−525.
(35) Vagin, A. A., and Isupov, M. N. (2001) Spherically averaged phased translation function and its application to the search for molecules and fragments in electron-density maps. *Acta Crystallogr. D57*, 1451−1456.
(36) Perrakis, A., Morris, R., and Lamzin, V. S. (1999) Automated protein model building combined with iterative structure refinement. *Nat. Struct. Biol. 6*, 458−463.
(37) Murshudov, G. N., Vagin, A. A., and Dodson, E. J. (1997) Refinement of macromolecular structures by the maximum-likelihood method. *Acta Crystallogr. D53*, 240−255.
(38) Emsley, P., and Cowtan, K. (2004) Coot: Model-building tools for molecular graphics. *Acta Crystallogr. D60*, 2126−2132.
(39) Winn, M. D., Isupov, M. N., and Murshudov, G. N. (2001) Use of TLS parameters to model anisotropic displacements in macromolecular refinement. *Acta Crystallogr. D57*, 122−133.
(40) Davis, I. W., Murray, L. W., Richardson, J. S., and Richardson, D. C. (2004) MOLPROBITY: Structure validation and all-atom contact analysis for nucleic acids and their complexes. *Nucleic Acids Res. 32*, W615−W619.
(41) Pettersen, E. F., Goddard, T. D., Huang, C. C., Couch, G. S., Greenblatt, D. M., Meng, E. C., and Ferrin, T. E. (2004) UCSF Chimera: A visualization system for exploratory research and analysis. *J. Comput. Chem. 25*, 1605−1612.
(42) Morris, G. M., Huey, R., Lindstrom, W., Sanner, M. F., Belew, R. K., Goodsell, D. S., and Olson, A. J. (2009) AutoDock4 and AutoDockTools4: Automated docking with selective receptor flexibility. *J. Comput. Chem. 30*, 2785−2791.
(43) Iovane, E., Giabbai, B., Muzzolini, L., Matafora, V., Fornili, A., Minici, C., Giannese, F., and Degano, M. (2008) Structural basis for substrate specificity in group I nucleoside hydrolases. *Biochemistry 47*, 4418−4426.
(44) Garau, G., Muzzolini, L., Tornaghi, P., and Degano, M. (2010) Active site plasticity revealed from the structure of the enterobacterial N-ribohydrolase RihA bound to a competitive inhibitor. *BMC Struct. Biol. 10*, 14.
(45) Degano, M., Gopaul, D. N., Scapin, G., Schramm, V. L., and Sacchettini, J. C. (1996) Three-dimensional structure of the inosine-uridine nucleoside N-ribohydrolase from *Crithidia fasciculata*. *Biochemistry 35*, 5971−5981.
(46) Degano, M., Almo, S. C., Sacchettini, J. C., and Schramm, V. L. (1998) Trypanosomal nucleoside hydrolase. A novel mechanism from the structure with a transition-state inhibitor. *Biochemistry 37*, 6277−6285.
(47) Fornili, A., Giabbai, B., Garau, G., and Degano, M. (2010) Energy Landscapes Associated with Macromolecular Conformational Changes from Endpoint Structures. *J. Am. Chem. Soc. 132*, 17570−17577.
(48) Versees, W., Loverix, S., Vandemeulebroucke, A., Geerlings, P., and Steyaert, J. (2004) Leaving group activation by aromatic stacking: An alternative to general acid catalysis. *J. Mol. Biol. 338*, 1−6.
(49) Gopaul, D. N., Meyer, S. L., Degano, M., Sacchettini, J. C., and Schramm, V. L. (1996) Inosine-uridine nucleoside hydrolase from *Crithidia fasciculata*. Genetic characterization, crystallization, and identification of histidine 241 as a catalytic site residue. *Biochemistry 35*, 5963−5970.
(50) Versees, W., Barlow, J., and Steyaert, J. (2006) Transition-state complex of the purine-specific nucleoside hydrolase of *T. vivax*: Enzyme conformational changes and implications for catalysis. *J. Mol. Biol. 359*, 331−346.
(51) Horenstein, B. A., Parkin, D. W., Estupinan, B., and Schramm, V. L. (1991) Transition-state analysis of nucleoside hydrolase from *Crithidia fasciculata*. *Biochemistry 30*, 10788−10795.